Research Square

Preprints are preliminary reports that have not undergone peer review. They should not be considered conclusive, used to inform clinical practice, or referenced by the media as validated information.

Termination controlled Phase-Pure Ti3C2Tx MXenes Towards Efficient Electrocatalysis

Simantini Nayak

simantini.immt@csir.res.in

CSIR-Institute of Minerals and Materials Technology https://orcid.org/0000-0002-0105-9771

Gyanprakash Mishra

CSIR-Institute of Minerals and Materials Technology

Saswati Mishra

CSIR-Institute of Minerals and Materials Technology

Brijesh Patel

Tata Institute of Fundamental Research

Satyabrata Sahoo

CSIR-Institute of Minerals and Materials Technology

Ashutosh Rath

CSIR-IMMT https://orcid.org/0000-0003-2559-9921

Article

Keywords:

Posted Date: October 15th, 2026

DOI: https://doi.org/10.21203/rs.3.rs-11201671/v1

License: This work is licensed under a Creative Commons Attribution 4.0 International License. Read Full License

Additional Declarations: There is **NO** Competing Interest.

Termination controlled Phase-Pure $Ti_3C_2T_x$ MXenes Towards Efficient Electrocatalysis

Gyanprakash Mishra,[1,2,3] Saswati Mishra,[1,3] Brijesh K. Patel,[4] Satyabrata Sahoo,[1,3] Ashutosh Rath,*[2,3] Simantini Nayak,*[1,3]

[1]Department of Materials Chemistry and Interfacial Engineering, CSIR-Institute of Minerals and Materials Technology, Bhubaneswar 751013, India

[2]Department of Mineralogy and Materials Characterisation, CSIR-Institute of Minerals and Materials Technology, Bhubaneswar 751013, India

[3]Academy of Scientific and Innovative Research (AcSIR), Gaziabad 201002, India

[4]Tata Institute of Fundamental Research, 36/P, Gopanpally Village, Hyderabad 500046, India

*Email: ashutosh.immt@csir.res.in
*Email: simantini.immt@csir.res.in

Abstract: MXenes are promising electrocatalysts for sustainable hydrogen generation, but establishing reliable structure–activity relationships to achieve phase purity and control surface terminations remains challenging. Here, we report phase-pure Ti_3C_2-F and Ti_3C_2-O MXenes synthesised via a molten-salt process, achieving purities >99.6%. Ti_3C_2-F exhibits excellent performance in the hydrogen evolution reaction (HER) in acidic solutions, with a very low overpotential of 86 mV at 10 mA cm^{-2} and a Tafel slope of 55 mV dec^{-1}. Ti_3C_2-O shows bifunctional catalytic activity in alkaline conditions, with HER and oxygen evolution reaction (OER) overpotentials of 76 and 134 mV at 10 mA cm^{-2}, and Tafel slopes of 86 and 102 mV dec^{-1}, respectively. Their outstanding activities and stabilities are attributed to phase-purity and tunable surface terminations, enabling different pathways for hydrogen and hydroxide activation. These findings not only elucidate the underlying reaction mechanisms but also demonstrate the potential of termination-controlled MXenes for efficient energy conversion.

MXenes, as emerging two-dimensional (2D) materials, have attracted considerable interest as efficient, cost-effective alternatives to noble-metal-based electrocatalysts for water splitting and hydrogen generation, owing to their high electrical conductivity, electrochemical stability, large surface area, and chemically active interfaces. MXenes are transition-metal compounds with the chemical formula $M_{n+1}X_nT_x$, synthesised by selectively removing the element A from 3D MAX ($M_{n+1}AX_n$) phases, where M stands for transition metals, X is C and/or N, A represents a group 13 or 14 element, and T_x is a surface functional group (-OH, -O, -Cl, -Br, or -F), with n = 1–3.[1–7] The electrocatalytic performance of MXenes is significantly influenced by their structural and morphological configuration, phase purity, and surface functional groups. Achieving high phase-purity MXene remains a challenge, as conventional MXene synthesis relies on strong-acid etching, viz., conc. Hydrofluoric acid, to etch the A layer of MAX phases.[8–10] During the etching process, the MAX phase is oxidised, resulting in impurities including residual MAX phase, metal oxides, terminal functional groups, and carbonaceous residues. Moreover, the phase purity, structural integrity, and interlayer spacing of MXenes are directly influenced by the structure and crystallinity of the respective MAX phase.[11–13] MXene-based layered materials are prone to sheet restacking due to van der Waals forces between attached functional groups, which narrow the interlayer spacing and reduce the number of accessible surface-active sites for electron transfer, thereby reducing electrochemical performance.[14–16] Most reported MXene-based systems provide indirect insights into synthesis routes, surface terminations, oxidation/impurity control, degradation kinetics, and film/electrode conductivity during hydrogen evolution reaction (HER)/oxygen evolution reaction (OER) activity.[8,17–19] However, a detailed quantitative understanding of the phase purity of MXene materials relative to their respective MAX phases and its direct correlation with HER/OER performance remains underexplored. Most MXene-based systems are synthesised using commercial MAX phases and other 'MXene-based' bifunctional catalysts (e.g. $RuCo_2O_4/Ti_3C_2T_x$, LDH/MXene, Co/Ni dual atoms on MXene, NiCoP on MXene, etc.), which primarily utilise MXene as a conductive scaffold material, where the real electron transfer centres during HER/OER reside in oxides, layered double hydroxides (LDHs), phospholipids, dual-atom sites, etc.[20–32]

The formation of a phase-pure MAX phase is a time-consuming, multistep process involving ball milling, pelletisation, high-temperature sintering of precursors under an inert atmosphere, pulverisation, and post-acid treatment.[13,15,33–39] Several strategies have been used to synthesise MAX phases at elevated temperatures, including hot pressing, spark plasma sintering, arc melting, and molten salt-shielded synthesis (MS^3).[36,37,40–42] In the MS^3 approach, molten salts create a shielding environment that minimises oxygen diffusion and surface oxidation at high temperatures. This enhances mass transport and reaction kinetics, facilitating phase formation and improving the crystallinity of the resulting MAX phase. The MS^3 method has been widely used to synthesise Ti_3SiC_2 and Ti_2AlN MAX phases.[43] However, the synthesis of phase-pure MAX phases remains under-explored. Only a few studies have reported MAX phase purities of 88% to 99% after high-temperature sintering, without further

discussion of how purity affects the structure and crystallinity of the resulting MXene.[11,13,36–39,42,44] Zhang *et al*. described an HF-free, alkali-assisted hydrothermal process for producing 92% pure multilayer $Ti_3C_2T_x$ (T = –OH, –O) MXene for energy storage applications, but did not report correlations between phase purity and electrochemical performance.[45]

Herein, we synthesised a high-phase-pure Ti_3AlC_2 MAX phase (purity: 99.45%) via MS^3 process and controlled-surface-terminated 2D $Ti_3C_2T_x$ (F-terminated; Ti_3C_2-F and O-terminated; Ti_3C_2-O) MXenes via HF-free etching, achieving purities of 99.6% to 99.7%. We systematically optimised synthesis parameters, including the initial precursor ratio, reaction temperature, reaction duration, and the etching process, to obtain high phase-pure MXenes. We further investigated the effect of surface terminations of $Ti_3C_2T_x$ MXene on overpotential, HER/OER activity and stability by tuning their surface functional groups (-F, -Cl, -O, -OH) using molten salt-assisted ($CuCl_2$, KCl and NaCl mixture) and *in-situ* HF etching (LiF dissolved in HCl) of the Ti_3AlC_2 MAX phase. Our results demonstrate that high-phase-pure Ti_3AlC_2 and HF-free etching produced Ti_3C_2-F and Ti_3C_2-O MXenes with high phase purity, controlled surface terminations, numerous exposed active sites, and enhanced catalytic activity and stability of the developed $Ti_3C_2T_x$ MXene for HER/OER in both acidic and alkaline media. We propose mechanistic pathways for HER and OER in Ti_3C_2-F and Ti_3C_2-O MXenes and show that phase purity and the presence of distinct surface functional groups are crucial in enhancing their electrocatalytic performance without any additional dopants or support materials.

Synthesis and characterisation of Ti_3AlC_2 MAX phase, Ti_3C_2-F and Ti_3C_2-O MXenes

We synthesised the Ti_3AlC_2 MAX phase via the MS^3 route by mixing elemental precursors Ti, TiC and Al in different molar ratios, according to the formula 2TiC: (1+a) Ti: (1+b) Al (where a = 0.1, 0.2, 0.25 and b = 0.4, 0.8, 1.2) (**Supplementary Table 5**), and sintering at 1200-1350 °C in air for 1 to 4 h. We systematically varied reaction parameters, such as sintering temperature, time, and precursor ratios, to achieve a high-phase-pure Ti_3AlC_2 MAX phase. Furthermore, we varied synthesis parameters, including sintering temperature, time, and precursor ratios, to evaluate the optimised conditions for the formation of the high-phase MAX phase (**Supplementary Fig. 1-3**). We prepared high-phase-pure 2D Ti_3C_2-F and Ti_3C_2-O MXenes via an HF-free etching process (**Fig. 1, Extended Data Fig. 1**) that removed the Al layers. We developed 2D Ti_3C_2-F MXene through *in-situ* HF etching by dissolving the as-prepared Ti_3AlC_2 MAX phase in a mixture of LiF in 9 M HCl at room temperature (RT) and 55 °C for 12 to 30 h under gentle stirring, and Ti_3C_2-O MXene by molten-salt etching of Ti_3AlC_2 at 700 °C for 6 to 24 h in the presence of a molten-salt mixture of $CuCl_2$, NaCl and KCl (**Supplementary Table 6**). In our approach, a >89-99% pure MAX phase was obtained without additional steps such as ball milling and pelletisation of raw materials and post-sintering acid washing of the MAX phase. Furthermore, no additional delamination step was required to obtain highly phase-pure (>99%) Ti_3C_2-

F and Ti_3C_2-O MXenes. The chemical reaction steps involved in the synthesis of the i) Ti_3AlC_2 MAX phase, ii) Ti_3C_2-F and iii) Ti_3C_2-O MXenes are represented by the following equations,

Reaction I

$$3Al_{(s)} + Ti_{(s)} \rightarrow Al_3Ti_{(s)} \quad (1)$$

$$Al_{(s)} \rightarrow Al_{(liq.)} \; air \rightarrow \; Al_2O_{3(s)} \quad (2)$$

$$Al_3Ti_{(s)} + TiC_{(s)} \rightarrow Ti_2AlC_{(s)} \quad (3)$$

$$Ti_2AlC_{(s)} + TiC_{(s)} \rightarrow Ti_3AlC_{2(s)} \quad (4)$$

Reaction II

$$LiF_{(s)} + HCl_{(aq.)} \rightarrow HF_{(aq.)} + LiCl_{(s)} \quad (5)$$

$$Ti_3AlC_{2(s)} + 3HF_{(aq.)} \rightarrow Ti_3C_{2(s)} + AlF_{3(s)} + \frac{3}{2}\, H_{2(g)}\uparrow \quad (6)$$

$$Ti_3C_{2(s)} + 2H_2O_{(aq.)} \rightarrow Ti_3C_2(OH)_{2(s)} + H_{2(g)}\uparrow \quad (7)$$

$$Ti_3C_{2(s)} + 2HF_{(aq.)} \rightarrow Ti_3C_2F_{2(s)} + H_{2(g)}\uparrow \quad (8)$$

Reaction III

$$Ti_3AlC_{2(s)} + \frac{3}{2}CuCl_{2(s)} \; air \rightarrow \; Ti_3C_2O + AlCl_{3(s)} + Al_2O_{3(s)} + \frac{3}{2}Cu_{(s)} \quad (9)$$

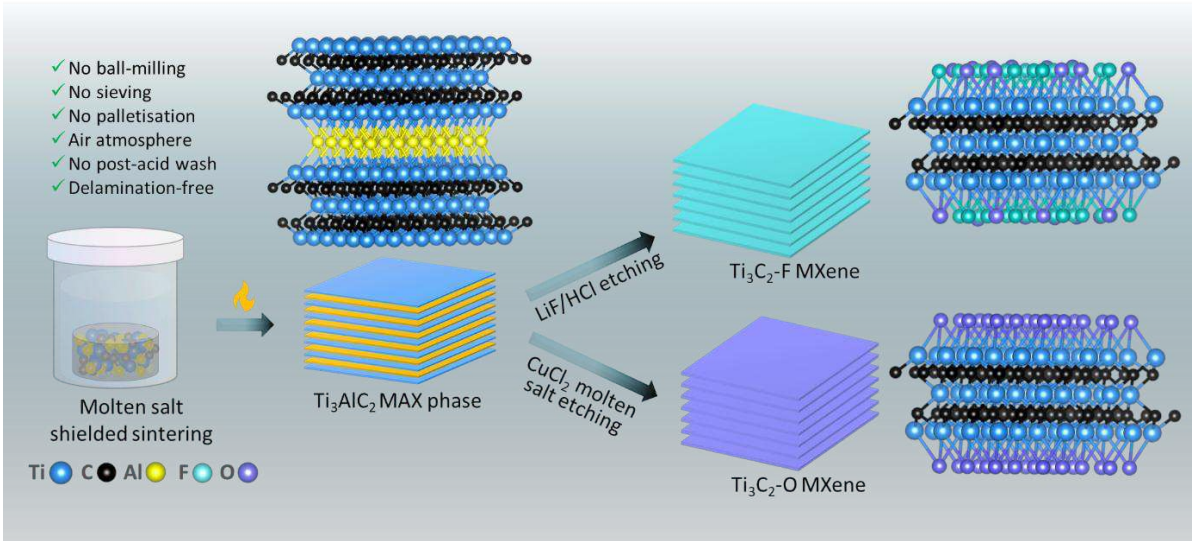

Fig. 1| Schematic illustration of the synthesis of the Ti_3AlC_2 MAX phase via molten-salt-shielded synthesis and of Ti_3C_2-F via *in situ* HF etching and Ti_3C_2-O via molten-salt etching.

The X-ray diffraction (XRD) patterns in **Fig. 2a** show the formation of the Ti_3AlC_2 MAX phase, with diffraction peaks at 39.06° and 9.5°, corresponding to the crystal planes (104) and (002), respectively and matching JCPDS card No. 00-052-0875. For Ti_3C_2-F MXene, the XRD pattern shows a major diffraction peak at 6.0º corresponding to the (002) crystal plane, the disappearance of the 39.06º peak, and a shift of the 9.5º peak to a lower angle (6.0º).[46] Similarly, for Ti_3C_2-O MXene, the peak at 39.06º

was absent, and the 9.5º peak shifted to 7.8º, indicating etching of the Al layers in the MAX phase.[16] An additional peak at 25.5º was observed for Ti_3C_2-O, corresponding to the (012) plane of Al_2O_3, indicating surface oxidation due to the higher temperature maintained during molten salt etching compared with the relatively lower temperature used for etching Ti_3C_2-F (55 ºC). The XRD pattern at 9.5º for the (002) plane shows an increase in d-spacing from 0.9 nm in Ti_3AlC_2 to 1.45 nm in Ti_3C_2-F and 1.13 nm in Ti_3C_2-O, further indicating the removal of Al layers and the formation of MXenes. Similarly, the Raman spectra (**Fig. 2b**) reveal peaks at 260, 410, and 611 cm^{-1} corresponding to the shear and longitudinal oscillations of Ti and Al atoms in the Ti_3AlC_2 MAX phase. For both Ti_3C_2-F and Ti_3C_2-O MXenes, the disappearance of the peak at 260 cm^{-1}, corresponding to Al, further correlates with the removal of Al and the formation of MXenes.[14] Two new peaks at 156 cm^{-1} and 203 cm^{-1} were also observed for both MXenes, corresponding to the E_g and A_{1g} modes of bare Ti_3C_2.[47,48]

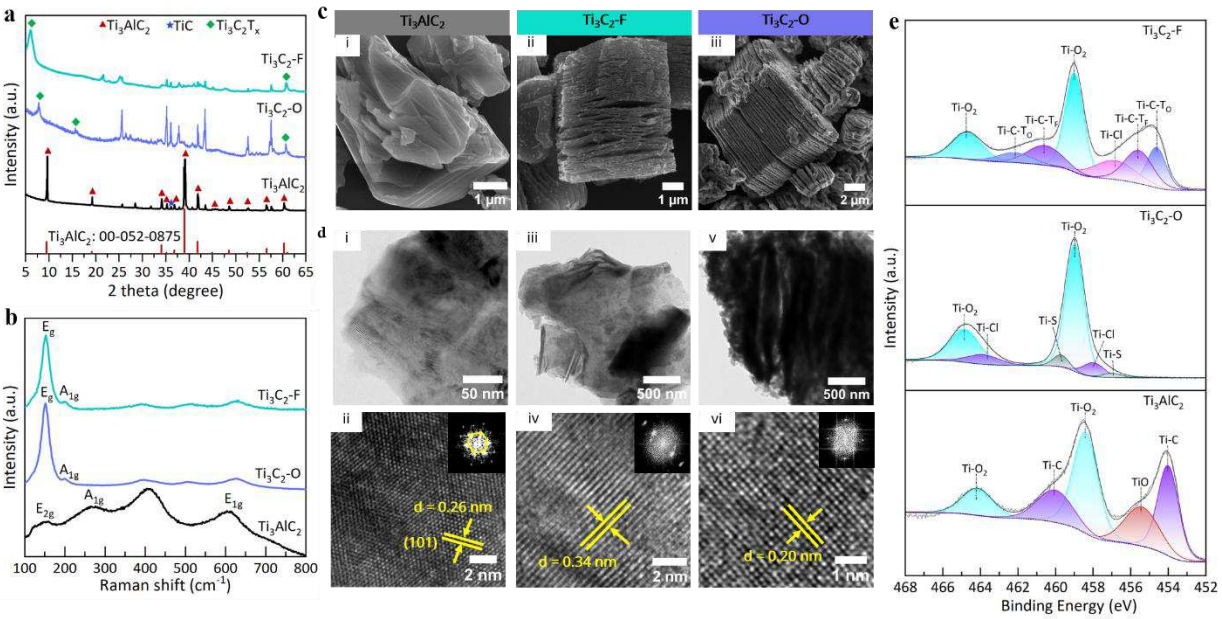

Fig. 2| Morphological and structural characterisations of Ti_3AlC_2 MAX phase and $Ti_3C_2T_x$ MXenes. **a**, XRD patterns. **b**, Raman spectra. **c**, FESEM images. **d**, TEM images. **e**, XPS Ti 2p spectra.

The phase purities of the Ti_3AlC_2 MAX phase and $Ti_3C_2T_x$ MXenes, with varied synthesis parameters (**Supplementary Table 5**), were calculated using the formula given in the experimental section. We found that, for high-phase-pure Ti_3AlC_2 MAX phase formation, Ti, TiC, and Al are required in a molar ratio of 1.25:2:2.2 at a sintering temperature of 1300 °C for 4 h. Etching of the high-phase-pure Ti_3AlC_2 MAX phase was carried out via *in-situ* HF and molten-salt etching routes at different reaction temperatures and times (**Supplementary Table 6**). For *in-situ* HF etching at room temperature for 24 h, only 30.70% phase-pure Ti_3C_2-F MXene was formed (**Supplementary Fig. 5**). Upon increasing the etching temperature to 55 °C and varying the etching duration from 12 to 30 h, the phase purity of the Ti_3C_2-F MXene was highest at 24 h (99.71%) (**Supplementary Fig. 6**). For the molten-salt etching route, varying the etching duration from 12 to 24 h at 700 °C (**Supplementary Table 6**), yielded 99.66% phase-pure Ti_3C_2-O MXene after 12 h. However, extending the etching time to 24 h led to oxidation of

Ti_3C_2-O. XRD analysis (**Supplementary Fig. 6**) shows a peak at ~25.5°, corresponding to the (102) plane of Al_2O_3, while the peak at ~9.5°, assigned to the (002) plane of Ti_3C_2-O MXene, completely vanished. These findings show that for effective and complete molten-salt etching of the Ti_3AlC_2 MAX phase, a 12 h etching duration at 700 °C is preferable.

Surface morphological features of the Ti_3AlC_2 MAX phase, Ti_3C_2-F and Ti_3C_2-O MXenes were analysed using field-emission scanning electron microscopy (FESEM), transmission electron microscopy (TEM) (**Fig. 2**) and Energy-dispersive X-ray spectroscopy (EDS) with elemental mapping (**Extended Data Fig. 2**). For the Ti_3AlC_2 MAX phase, the FESEM image shows the formation of a compact multilayer structure, with EDS showing an Al at% of 8.1. Upon *in situ* HF etching of the MAX phase, well-spaced few-layer Ti_3C_2-F MXene was obtained with distinct interlayer spacings, consistent with complete Al removal. In contrast, molten salt-etched Ti_3C_2-O MXene formed multi-layered structures with comparatively larger interlayer spacings than Ti_3C_2-F (**Fig. 2d**). EDS measurements and elemental mapping show that the Al at% was reduced to 3.1% in Ti_3C_2-F and 2.7% in Ti_3C_2-O MXenes compared with 8.1% in the Ti_3AlC_2 MAX phase. Furthermore, the N_2 adsorption-desorption isotherms (**Supplementary Fig. 7**) of Ti_3C_2-F MXene showed a type-IV pattern with a specific surface area of ~8.18 ± 0.11 m^2/g, pore size distribution of 3-180 nm (mostly 5-30 nm) and a pore volume of 0.019 cm^3/g. In contrast, Ti_3C_2-O possesses a much larger accessible surface area and pore volume than Ti_3C_2-F, with a specific surface area of ~98.96 ± 0.40 m^2/g, a pore size of 1.5-221 nm (mostly 2-50 nm) and a pore volume of 0.1445 cm^3/g. Thermogravimetric–differential scanning calorimetry (TG-DSC analysis (**Supplementary Fig. 8**) showed Ti_3AlC_2 lost 5.83% weight below 400 °C due to moisture removal, then gained 29.74% from oxidation up to 1200 °C, forming Al_2O_3 and TiO_2. Ti_3C_2-O MXene exhibited a similar trend: 20.55% loss below 400 °C, then 32.35% gain up to 1200 °C, whereas Ti_3C_2-F showed 19.26% loss below 500 °C due to water removal, no change between 500–900 °C, and 4.85% loss from bound water up to 1200 °C. These results confirm that Ti_3C_2-F is thermally more stable up to 900 °C, with higher purity and lower oxide content. The high-resolution TEM and corresponding Fast Fourier Transform (FFT) images (inset) of the Ti_3AlC_2 MAX phase (**Fig. 2d (i) and (ii)**) also confirm the hexagonal crystal structure, with a d-spacing of 0.26 nm corresponding to the (101) plane. Similarly, for Ti_3C_2-F, the d-spacing increased to 0.34 nm for the same plane, reflecting structural expansion during *in situ* HF etching (**Fig. 2d (iii) and (iv)**). In contrast, Ti_3C_2-O show a reduced d-spacing of 0.20 nm (**Fig. 2d (v) and (vi)**).

We performed X-ray photoelectron spectroscopy (XPS) measurements to confirm the surface chemical composition and electronic states of the Ti_3AlC_2 MAX phase, Ti_3C_2-F and Ti_3C_2-O MXenes. The XPS survey spectra (**Supplementary Fig. 12**) show that the Ti_3AlC_2 MAX phase contains Ti 2p, Al 2p, and C 1s signals along with a strong O 1s signal, indicating partial surface oxidation of the MAX phase. The XPS survey spectra of both Ti_3C_2-F and Ti_3C_2-O MXenes formed after the etching process show that the Ti 2p peak intensity is enhanced, whereas the Al 2p peak intensity is weaker than in the Ti_3AlC_2

MAX phase. This confirms the successful removal of the Al layer and formation of the phase-pure MXenes. The Ti 2p spectra (**Fig. 2e, Supplementary Table 1**) show Ti-C, TiO_2, and Ti-O bonds in the Ti_3AlC_2 MAX phase, confirming partial surface oxidation and formation of the surface TiO_2. In Ti_3C_2-F MXene, the spectra reveal Ti-C-T_F and Ti-C-T_O bonds, confirming F/O surface functionalities, as well as Ti-Cl and TiO_2 states (**Supplementary Tables 2 and 3**). In contrast, Ti_3C_2-O primarily shows TiO_2 bonds, along with Ti-S and Ti-Cl, confirming oxygen-rich surface terminations. Overall, Ti 2p analysis shows that the etching process significantly alters MXene surface functionalization. The high-resolution O 1s spectrum (**Extended data Fig. 3a**) shows the presence of TiO_2, Al_2O_3, and surface hydroxyl group (-OH-Ti-O) species in the Ti_3AlC_2 MAX phase, whereas Ti_3C_2-F and Ti_3C_2-O MXenes show a dominant C-Ti-O_x environment and adsorbed H_2O species, with residual oxidised impurities such as TiO_2, predominant in Ti_3C_2-F MXene, and Al_2O_3 in Ti_3C_2-O MXene, arising from their respective etching methods.

Electrochemical universal pH HER performance

To investigate the electrochemical HER activity of high-phase-pure Ti_3C_2-F and Ti_3C_2-O MXenes, we evaluated both the catalysts in acidic (0.5 M H_2SO_4) and alkaline (1 M KOH) electrolytes (**Fig. 3**). Linear sweep voltammetry (LSV) results show both the catalysts exhibit excellent HER performance at high current densities (up to 1300 mA cm^{-2} for Ti_3C_2-F at acidic pH and 1240 mA cm^{-2} for Ti_3C_2-O at alkaline pH) compared to the state-of-the art 10% Pt/C catalyst. Notably, the Ti_3C_2-F demonstrates the highest activity in acidic medium, outperforming Ti_3C_2-O. At 10 mA cm^{-2}, Ti_3C_2-F shows an overpotential (η) of 86 mV, which is ~20 mV lower than that of Ti_3C_2-O MXene (**Fig. 3a**). Both MXenes exhibit overpotentials (η) comparable to those of the benchmark commercial 10% Pt/C catalyst (η = 73 mV), indicating superior HER activity in acidic media. In contrast, Ti_3C_2-O exhibits the highest HER performance in 1 M KOH compared to Ti_3C_2-F and the state-of-the-art 10% Pt/C (**Fig. 3b**). At 10 mA cm^{-2}, Ti_3C_2-O shows an overpotential of 76 mV, which is notably 21 mV lower than that of 10% Pt/C. Ti_3C_2-F shows a lower Tafel slope of 55 mV dec^{-1} at acidic pH, while Ti_3C_2-O has a lower slope of 86 mV dec^{-1} at alkaline pH (**Fig. 3d**). The Tafel slope analysis indicates that HER kinetics mainly follow the Volmer-Heyrovsky mechanism, with surface chemistry governing the adsorption and desorption steps. To further elucidate the interfacial charge-transfer kinetics, we performed electrochemical impedance spectroscopy (EIS) measurements (**Supplementary Fig. 16**). Ti_3C_2-F exhibits a lower R_s of 0.76 Ω and an R_{ct} of 20.12 Ω at acidic pH, while Ti_3C_2-O shows reduced R_s (2.06 Ω) and R_{ct} (61.8 Ω) at alkaline pH. This indicates that charge-transfer kinetics are pH-dependent: Ti_3C_2-F is more efficient under acidic conditions, whereas Ti_3C_2-O is more efficient under alkaline conditions. Moreover, in acidic medium, Ti_3C_2-F shows an exceptionally high electrochemically active surface area (ECSA) of 563.14 cm^2 and a roughness factor of 2252.56, surpassing Ti_3C_2-O (**Supplementary Table 7 and Supplementary Fig. 14**). Remarkably, Ti_3C_2-F maintained stable operation for over 39 h at a high current density of 260 mA cm^{-2} at -0.54 V vs RHE, and 9000 CV cycles at acidic pH (**Fig. 3e (i)**)

whereas Ti_3C_2-O exhibits stable operation over 19 h at 200 mA cm ^{2} at -0.43 V vs RHE, and 2100 CV cycles (**Fig. 3e (ii)**) as evidenced by chronoamperometry, cyclic voltammetry measurements as well as post-mortem morphological and chemical characterisations (**Supplementary Figs. 17–21**). The Faradaic efficiency (FE) of Ti_3C_2-F exceeded 99% after 34 h but dropped to 87% at 39.5 h at acidic pH, while Ti_3C_2-O maintained 98% FE after 19 h, at alkaline pH.

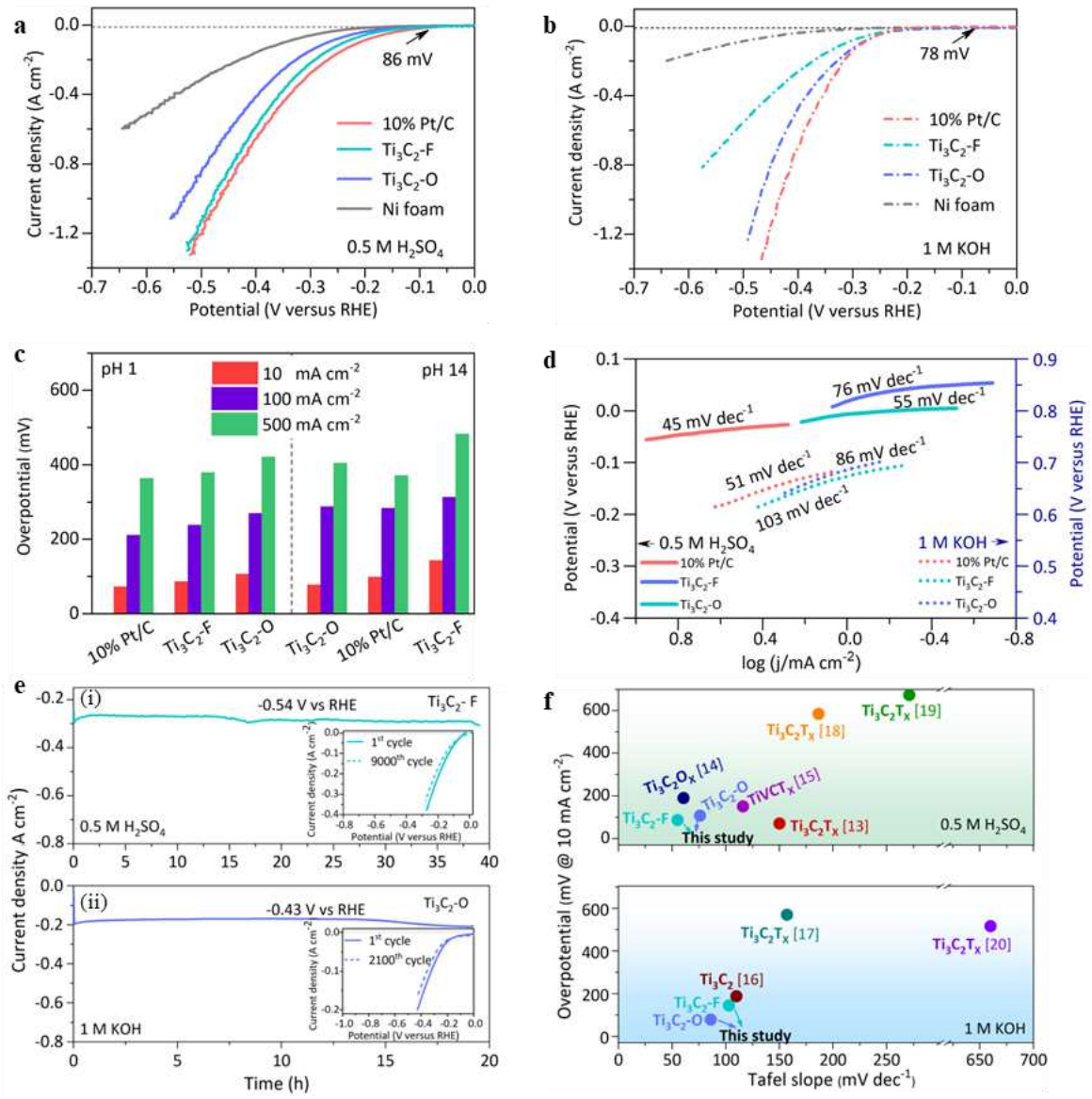

Fig. 3| Electrochemical HER performance. LSV curves of Ti_3C_2-F and Ti_3C_2-O at a scan rate of 5 mV s^{-1}; **a**, in 0.5 M H_2SO_4, **b**, in 1 M KOH. **c**, Comparison of overpotentials at 10 mA cm^{-2}, 100 mA cm^{-2}, 500 mA cm^{-2}. **d**, Tafel plots. **e**, Chronoamperometry and cyclic voltammetry stability (inset) measurements of **(i)** Ti_3C_2-F in 0.5 M H_2SO_4, **(ii)** Ti_3C_2-O in 1 M KOH. **f**, Comparison of overpotentials and Tafel slopes with reported titanium-carbide-based MXenes as HER electrocatalysts.

Electrochemical OER and overall water splitting performance

sTo further examine the bifunctional electrocatalytic ability of the synthesized catalyst, we tested the OER performance of Ti_3C_2-F and Ti_3C_2-O in 1 M KOH (**Fig. 4**). The LSV results show that Ti_3C_2-O exhibits excellent OER activity, with an overpotential of 134 mV at 10 mA cm^{-2}, just 13 mV less than Ti_3C_2-F, indicating similar OER performance between the two MXenes (**Fig. 4b**). Consistent with the LSV data, Ti_3C_2-O displays much faster OER kinetics, evidenced by a lower Tafel slope of 102 mV dec^{-1} compared to 110 mV dec^{-1} for Ti_3C_2-F (**Fig. 4c**). Additionally, Ti_3C_2-O has a higher C_{dl} of 3.84 mF cm^{-2} versus 2.29 mF cm^{-2} for Ti_3C_2-F, suggesting more active sites are exposed. The higher C_{dl}, ESCA, and roughness factor of Ti_3C_2-O compared to Ti_3C_2-F point to improved charge-transfer activity, thereby enhancing OER kinetics under alkaline conditions (**Supplementary Fig. 15, Table 7**). Ti_3C_2-O maintained excellent OER stability over 19.2 hours, with a steady current at +1.87 V versus RHE and 2100 cycles without notable degradation, as evidenced by chronoamperometry and CV measurements (**Fig. 4d (i)**) as well as post-mortem morphological and chemical characterisations (**Supplementary Figs. 19 and 20**). Additionally, to assess the practical potential of the Ti_3C_2-O catalyst, we evaluated its overall water-splitting performance in a two-electrode setup**.** The symmetric Ti_3C_2-O || Ti_3C_2-O cell delivered excellent performance in 1 M KOH, requiring only +1.75 V to reach a current density of 20 mA cm^{-2} (**Fig. 4d (ii)**). The system remained stable for over 42 h at this voltage, confirming robust long-term water-splitting stability (**Fig. 4f**). These results demonstrate the high bifunctional electrocatalytic activity of Ti_3C_2-O under alkaline conditions for overall water splitting.

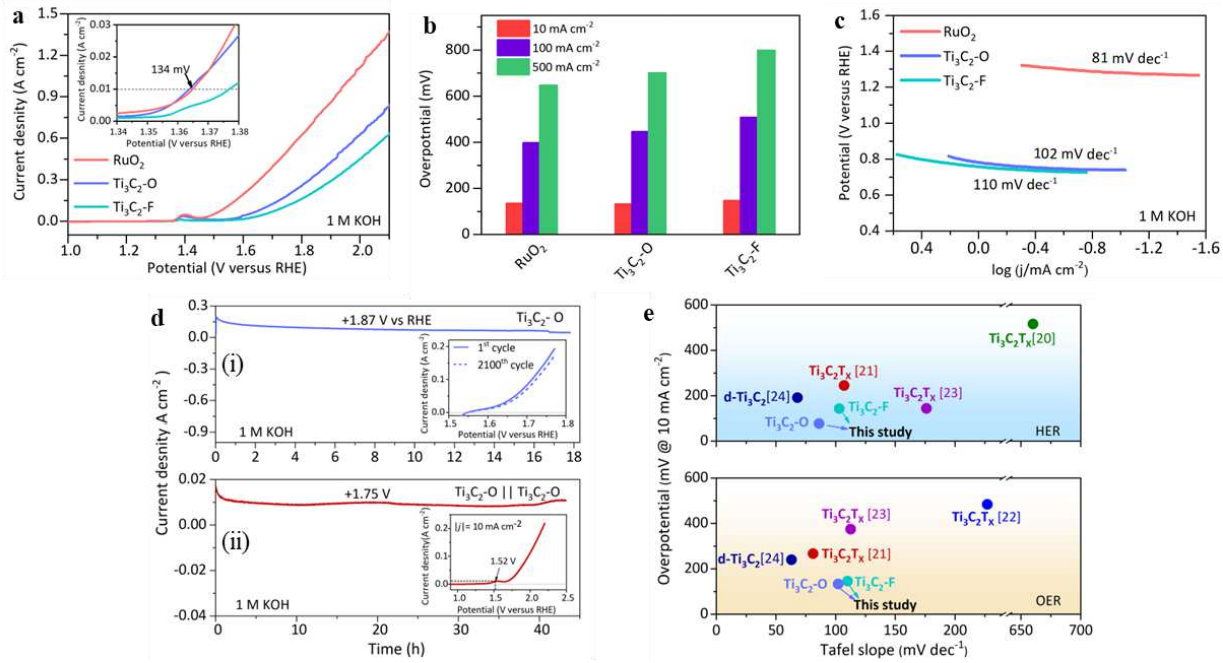

Fig. 4| Electrochemical OER performance. a, LSV curves of Ti_3C_2-F and Ti_3C_2-O in 1 M KOH at a scan rate of 5 mV s^{-1}. **b**, Comparison of overpotentials at 10 mA cm^{-2}, 100 mA cm^{-2} and 500 mA cm^{-2}. **c**, Tafel plots. **d, (i)** Chronoamperometry and cyclic voltammetry stability (inset) measurements of Ti_3C_2-O in 1 M KOH. **(ii)** Chronoamperometry and LSV curve (inset) of overall water splitting for two-electrode Ti_3C_2-O || Ti_3C_2-O in 1 M KOH. **e**, Comparison of overpotentials and Tafel slopes in reported titanium-carbide-based MXenes as OER electrocatalysts.

Mechanistic insights into electrocatalytic performance

All the above-mentioned electrocatalytic results for Ti_3C_2-F and Ti_3C_2-O MXenes show distinct pH-dependent HER activity in both 0.5 M H_2SO_4 and 1 M KOH, and OER performance indicating bifunctional water splitting in 1 M KOH. The superior HER activity of Ti_3C_2-F at acidic pH could be attributed to the presence of dual surface functionalities, -F (25.65 at%) and -O (23.13 at%), as confirmed by XPS analysis (**Supplementary Table 4**). The proposed HER mechanism on the Ti_3C_2-F surface in an acidic medium is shown in **Fig. 5a**; Ti-O groups serve as the primary H^+ adsorption sites, forming Ti-O--H intermediates, while adjacent -F terminations electronically modulate these active centres, without directly participating in H^+ binding.[49] This synergistic effect facilitates rapid H^+ adsorption/desorption, lowering the overpotential and accelerating HER kinetics of Ti_3C_2-F compared to Ti_3C_2-O at acidic pH.

In contrast, in an alkaline medium, the superior bifunctional water-splitting activity of Ti_3C_2-O may be attributed to the predominance of the -O functional group (52.63 at% as confirmed by XPS analysis, **Supplementary Table 4**). The proposed HER and OER mechanisms on the Ti_3C_2-O surface in an alkaline medium are shown in **Fig. 5b and 5c**. For HER, water molecules in the KOH solution serve as the H^+ source, owing to the scarcity of free protons relative to those in acidic solutions. Ti-O sites promote water adsorption and subsequently facilitate O-H bond weakening via interfacial charge redistribution, accelerating H_2O dissociation to form H_{ads} and OH^- species (Volmer step) and rapid H* generation. This scheme reduces the overpotential and accelerates HER kinetics of Ti_3C_2-O at alkaline pH. For OER, OH^- ions are adsorbed on Ti-O active sites to form OH^*, O* and OOH* intermediates via efficient charge transfer during sequential deprotonation and O-O bond formation, thereby lowering the OER overpotential and accelerating the kinetics, enhancing the overall OER performance. In comparison, the fluoride-rich Ti_3C_2-F catalyst surface is less favourable at alkaline pH as -F terminations don't efficiently promote H_2O dissociation during HER nor stabilise oxygenated intermediates during OER.

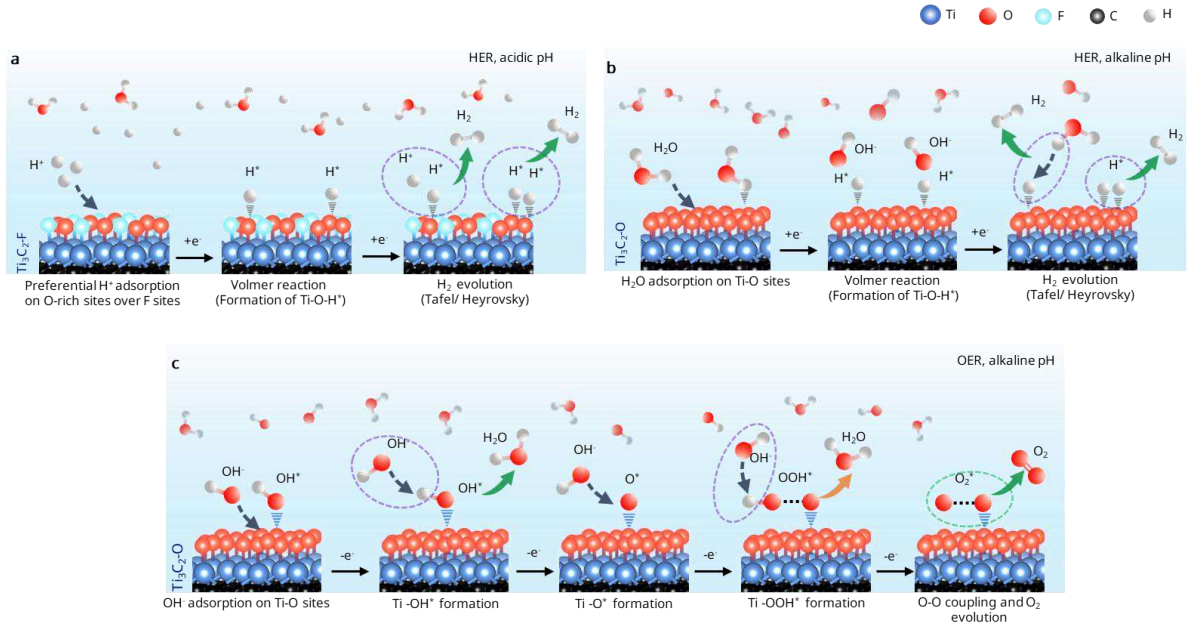

Fig. 5| Proposed mechanism schemes of HER and OER. a, HER on the Ti_3C_2-F surface in 0.5 M H_2SO_4; **b**, HER on the Ti_3C_2-O surface in 1 M KOH; **c**, OER on the Ti_3C_2-O surface in 1 M KOH.

Conclusion

In summary, a simple molten-salt-assisted synthesis combined with HF-free etching produced phase-pure Ti_3C_2-F and Ti_3C_2-O MXenes with purities exceeding 99.66%. Their distinct surface terminations provide abundant active sites, promote efficient charge transport, and tune the electronic structure and reaction kinetics. Ti_3C_2-F exhibited excellent HER activity in acidic media, with low overpotential and operational stability for more than 40 h. This performance is attributed to the synergistic effect of the -F and -O surface functionalities, where O-containing sites primarily serve as hydrogen adsorption sites, while the electronegative -F terminations regulate the surface electronic structure and the hydrogen adsorption/desorption process. Similarly, Ti_3C_2-O MXene exhibited remarkable bifunctional electrocatalytic activity in alkaline media, delivering overall water-splitting performance comparable to the benchmark catalysts. This superior activity is due to the oxygen-rich C-Ti-O_x surface environment, which enhances OH^- activation and accelerates reaction kinetics. An outstanding Faradaic efficiency of >99% was achieved for Ti_3C_2-F MXene, while Ti_3C_2-O delivered ~90%, confirming highly efficient and selective hydrogen production. The synthesis method can be extended to synthesise phase-pure MXenes from other transition metals, including Mo, V, and Cr, opening a path to explore highly effective phase-pure MXenes for a range of renewable-energy applications beyond water splitting.

Online content

Any methods, additional references, Nature Portfolio reporting summaries, source data, extended data, supplementary information, acknowledgements, peer-review information, details of author contributions and competing interests, and statements of data and code availability are available at https://doi.org/10.1038/xxx.

References

1. Naguib, M., Barsoum, M. W. & Gogotsi, Y. Ten Years of Progress in the Synthesis and Development of MXenes. *Advanced Materials* **33**, (2021).

2. Naguib, M., Mochalin, V. N., Barsoum, M. W. & Gogotsi, Y. 25th anniversary article: MXenes: A new family of two-dimensional materials. *Advanced Materials* **26**, 992–1005 (2014).

3. Naguib, M. *et al.* Two-dimensional transition metal carbides. *ACS Nano* **6**, 1322–1331 (2012).

4. Gogotsi, Y. & Anasori, B. The Rise of MXenes. *ACS Nano* **13**, 8491–8494 (2019).

5. Michałowski, P. P. *et al.* Oxycarbide MXenes and MAX phases identification using monoatomic layer-by-layer analysis with ultralow-energy secondary-ion mass spectrometry. *Nat. Nanotechnol.* **17**, 1192–1197 (2022).

6. Han, M. *et al.* Electrochemically modulated interaction of MXenes with microwaves. *Nat. Nanotechnol.* **18**, 373–379 (2023).

7. Liu, S. *et al.* Hydrogen storage in incompletely etched multilayer Ti_2CT_x at room temperature. *Nat. Nanotechnol.* **16**, 331–336 (2021).

8. Zhang, C. (John) *et al.* Additive-free MXene inks and direct printing of micro-supercapacitors. *Nat. Commun.* **10**, (2019).

9. Thakur, A. *et al.* Step-by-Step Guide for Synthesis and Delamination of $Ti_3C_2T_x$ MXene. *Small Methods* **7**, (2023).

10. Shuck, C. E. *et al.* Safe Synthesis of MAX and MXene: Guidelines to Reduce Risk during Synthesis. *ACS Chemical Health and Safety* **28**, 326–338 (2021).

11. Choudhary, E., Manjunath, V., Kalubarme, R., Jangir, R. & Devan, R. S. Molten salt-shielded solid-state synthesis (MS5) reaction-driven >99% pure Ti_3AlC_2 MAX phase: effect of MAX phase purity on the interlayer separation of MXenes and Na-ion storage. *Nanoscale* **16**, 17599–17615 (2024).

12. Choudhary, E. *et al.* MAX Phase Purity Contingent Interlayer Spacing Regulated Ti_3C_2-F MXene Electrodes for Efficient Energy Storage Application. *Small* **21**, (2025).

13. Shuck, C. E. *et al.* Effect of Ti3AlC2 MAX Phase on Structure and Properties of Resultant $Ti_3C_2T_x$ MXene. *ACS Appl. Nano Mater.* **2**, 3368–3376 (2019).

14. Sharma, P., Kainth, S., Pandey, O. P. & Mahajan, R. Customized Synthesis of 2D Ti_3C_2 MXene for Improved Overall Water Splitting. *ACS Appl. Nano Mater.* **6**, 21788–21802 (2023).

15. Mathis, T. S. *et al.* Modified MAX Phase Synthesis for Environmentally Stable and Highly Conductive Ti_3C_2 MXene. *ACS Nano* **15**, 6420–6429 (2021).

16. Mashtalir, O., Naguib, M., Dyatkin, B., Gogotsi, Y. & Barsoum, M. W. Kinetics of aluminum extraction from Ti_3AlC_2 in hydrofluoric acid. *Mater. Chem. Phys.* **139**, 147–152 (2013).

17. Chen, J. *et al.* Progress in MXene-based catalysts for oxygen evolution reaction. *Electron* **2**, (2024).

18. Ran, J. *et al.* Ti_3C_2 MXene co-catalyst on metal sulfide photo-absorbers for enhanced visible-light photocatalytic hydrogen production. *Nat. Commun.* **8**, (2017).

19. Guo, D. *et al.* A dual-active Co-CoO heterojunction coupled with Ti_3C_2-MXene for highly-performance overall water splitting. *Nano Res.* **15**, 238–247 (2022).

20. Zhang, R., Zhou, Y., Yue, Q. & Kang, Y. Electro catalytic Performance of bimetallic LDH on Mxene Adsorbed Nickle Foam. in *IOP Conference Series: Materials Science and Engineering* vol. 612 (Institute of Physics Publishing, 2019).

21. Li, Z., Wang, X., Ren, J. & Wang, H. NiFe LDH/$Ti_3C_2T_x$/nickel foam as a binder-free electrode with enhanced oxygen evolution reaction performance. *Int. J. Hydrogen Energy* **47**, 3886–3892 (2022).

22. Yu, M., Zheng, J. & Guo, M. La-doped NiFe-LDH coupled with hierarchical vertically aligned MXene frameworks for efficient overall water splitting. *Journal of Energy Chemistry* **70**, 472–479 (2022).

23. Zou, Y. *et al.* Ruthenium single-atom modulated $Ti_3C_2T_x$ MXene for efficient alkaline electrocatalytic hydrogen production. *EcoMat* **5**, (2023).

24. Zhang, X. *et al.* Platinum Nanoparticle-Deposited $Ti_3C_2T_x$ MXene for Hydrogen Evolution Reaction. *Ind. Eng. Chem. Res.* **59**, 1822–1828 (2020).

25. Zhu, J. *et al.* Anchoring isolated Pd atoms on $Ti_3C_2T_x$ MXene with boosted kinetics for alkaline hydrogen evolution. *Appl. Surf. Sci.* **644**, (2024).

26. Suragtkhuu, S. *et al.* Rhenium anchored $Ti_3C_2T_x$ (MXene) nanosheets for electrocatalytic hydrogen production. *Nanoscale Adv.* **5**, 349–355 (2022).

27. Yan, L., Chen, Y., Xie, J. & Li, H. Architecting Ni_3Se_4-$NiSe_2$-Co_3O_4 Triple-Interface Heterostructure on MXene Nanosheets for Boosting Water Splitting by Electronic Modulation and Interface Effects. *Small* **20**, (2024).

28. Zhang, B., Shan, J., Wang, X., Hu, Y. & Li, Y. Ru/Rh Cation Doping and Oxygen-Vacancy Engineering of FeOOH Nanoarrays@$Ti_3C_2T_x$ MXene Heterojunction for Highly Efficient and Stable Electrocatalytic Oxygen Evolution. *Small* **18**, (2022).

29. Wang, J. *et al.* MXene-Assisted NiFe sulfides for high-performance anion exchange membrane seawater electrolysis. *Nature Communications* **16**, (2025).

30. Zhang, X. *et al.* Hierarchical NiFeP Nanoflowers on the MXene Film as a Self-Standing Bifunctional Electrode toward Superior Overall Water Electrolysis. *ACS Appl. Nano Mater.* **7**, 7684–7693 (2024).

31. Lv, Z. *et al.* Induction of Co2P Growth on a MXene ($Ti_3C_2T_x$)-Modified Self-Supporting Electrode for Efficient Overall Water Splitting. *Journal of Physical Chemistry Letters* **12**, 4841–4848 (2021).

32. Kaplan, C. *et al.* Effect of the synthesis route and Co Coverage on Co / $Ti_3C_2T_x$ materials for the oxygen evolution reaction. *Electrochim. Acta* **490**, (2024).

33. Kotasthane, V. *et al.* Selective Etching of Ti_3AlC_2 MAX Phases Using Quaternary Ammonium Fluorides Directly Yields Ti_3C_2T MXene Nanosheets: Implications for Energy Storage. *ACS Appl. Nano Mater.* **6**, 1093–1105 (2023).

34. von Treifeldt, J. E. *et al.* The effect of Ti_3AlC_2 MAX phase synthetic history on the structure and electrochemical properties of resultant Ti_3C_2 MXenes. *Mater. Des.* **199**, (2021).

35. Placke, T. *et al.* Solvent co-intercalation into few-layered $Ti_3C_2T_x$ MXenes in lithium ion batteries induced by acidic or basic post-treatment. *ACS Nano* **15**, 3295–3308 (2021).

36. Feng, L., Lv, M., Qian, Q., Luo, R. & Huang, B. The synthesis of high purity Ti_3AlC_2 MAX phase via molten salt method. *Advanced Powder Technology* **34**, (2023).

37. Guan, K. *et al.* Efficient synthesis of Ti_3AlC_2 powders with high purity by microwave-assisted molten salt method. *Ceram. Int.* **48**, 16357–16363 (2022).

38. Liu, Y. *et al.* Facile synthesis of hollow Ti_3AlC_2 microrods in molten salts via Kirkendall effect. *Journal of Advanced Ceramics* **11**, 1491–1497 (2022).

39. Gao, L. *et al.* Preparation and performance of MAX phase Ti_3AlC_2 by in-situ reaction of Ti-Al-C system. *Advanced Powder Technology* **31**, 3533–3539 (2020).

40. Ma, G. *et al.* Li-ion storage properties of two-dimensional titanium-carbide synthesized via fast one-pot method in air atmosphere. *Nat. Commun.* **12**, (2021).

41. Hu, Z. *et al.* Rapid mass production of two-dimensional metal oxides and hydroxides via the molten salts method. *Nat. Commun.* **8**, (2017).

42. Bärmann, P. *et al.* Scalable Synthesis of MAX Phase Precursors toward Titanium-Based MXenes for Lithium-Ion Batteries. *ACS Appl. Mater. Interfaces* **13**, 26074–26083 (2021).

43. Dash, A., Vaßen, R., Guillon, O. & Gonzalez-Julian, J. Molten salt shielded synthesis of oxidation prone materials in air. *Nat. Mater.* **18**, 465–470 (2019).

44. Chen, B. *et al.* Subsize $Ti_3C_2T_x$ derived from molten-salt synthesized Ti_3AlC_2 for enhanced capacitive deionization. *Ceram. Int.* **47**, 3665–3670 (2021).

45. Li, T. *et al.* Fluorine-Free Synthesis of High-Purity $Ti_3C_2T_x$ (T=OH, O) via Alkali Treatment. *Angew. Chem. Int. Ed.* **57**, 6115–6119 (2018).

46. Anayee, M. *et al.* Kinetics of Ti_3AlC_2 Etching for $Ti_3C_2T_x$ MXene Synthesis. *Chemistry of Materials* **34**, 9589–9600 (2022).

47. Sarycheva, A. & Gogotsi, Y. Raman Spectroscopy Analysis of the Structure and Surface Chemistry of $Ti_3C_2T_x$ MXene. *Chemistry of Materials* **32**, 3480–3488 (2020).

48. Shevchuk, K., Sarycheva, A., Shuck, C. E. & Gogotsi, Y. Raman Spectroscopy Characterization of 2D Carbide and Carbonitride MXenes. *Chemistry of Materials* **35**, 8239–8247 (2023).

49. Meng, L., Yan, L. K., Viñes, F. & Illas, F. Effect of terminations on the hydrogen evolution reaction mechanism on Ti_3C_2 MXene. *J. Mater. Chem. A Mater.* **11**, 6886–6900 (2023).

Methods

Materials

Ti (325 mesh, 99.95%), TiC (99.5%), Al (325 mesh, 99.95%), $CuCl_2$ (98%) from Thermo Fisher Scientific, NaCl (98.5-102.0%), KCl (99.0-100.5%), HCl (35% v/v) from HiMedia Laboratories Pvt. Ltd., LiF (99.995%, Sigma Aldrich Chemicals Pvt. Ltd.) were used to synthesize the Ti_3AlC_2 MAX phase and $Ti_3C_2T_x$ MXene. Titanium aluminium carbide 312 commercial MAX Phase (>90%, 40 µm particle size) from Sigma Aldrich was used for comparison with the synthesised Ti_3AlC_2 MAX phase. Nickel foam (110 PPI, Eliteck), Aquivion® ionomer solution (25 wt%, Sigma Aldrich), H_2SO_4 (98% v/v, HiMedia Laboratories Pvt. Ltd.), and KOH (>85%, Tokyo Chemical Industry Co., Ltd.) were used for electrochemical measurements. All chemicals were used as received without further purification. Milli-Q water (18.2 MΩ · cm) was used for all experiments.

Synthesis of Ti_3AlC_2 MAX phase

For Ti_3AlC_2 MAX phase synthesis, we used a mixture of elemental precursors Ti, TiC and Al in different molar ratios, with the formula 2TiC: (1+a) Ti: (1+b) Al (where a = 0.1, 0.2, 0.25 and b = 0.4, 0.8, 1.2). The mixture was ground in a mortar and pestle for 0.5-1 h and transferred to an alumina crucible, which was placed in another large alumina crucible filled with a NaCl-KCl salt mixture at a 1:1 molar ratio and sealed with an alumina lid. The mixture was sintered at 1200-1400 °C for 1-4 h in air using a muffle furnace (Ants Innovation, India), without any inert gas protection. The furnace was allowed to cool naturally to room temperature, and the solid mixture was removed from the salt bed and washed 2-3 times with Milli-Q water to remove any residual salt. The black, compact sample was crushed with a mortar and pestle, and the Ti_3AlC_2 MAX-phase powder was collected, as shown in Extended Data Figure 1.

Synthesis of $Ti_3C_2T_x$ MXene

Using the synthesised Ti_3AlC_2 MAX phase, $Ti_3C_2T_x$ MXene was prepared via two routes: *in-situ* HF etching and molten-salt etching, as discussed below.

a) <u>Ti_3C_2-F MXene via *in-situ* HF etching</u>: Ti_3AlC_2 MAX powder was added to a mixture of LiF in 9 M HCl (mass-to-volume ratio 0.08 g/ml) at a MAX phase-to-LiF mass ratio of 1:1.6. The mixture was gently stirred at 55 °C for 12-30 h. The product was washed with Milli-Q water by centrifugation until the pH reached 6-7. The washed sample was then dried in an oven at 60 °C for 12-24 h, and the Ti_3C_2-F MXene powder was collected.

b) <u>Ti_3C_2-O MXene via molten salt etching</u>: To synthesise Ti_3C_2-O MXene by molten salt etching, we added Ti_3AlC_2 MAX phase powder to a molten salt mixture of $CuCl_2$, NaCl, and KCl in a molar ratio of 1:3:2:2 and ground the mixture with a mortar and pestle for 5-10 min. The mixture was transferred to an alumina crucible and placed within a larger alumina crucible filled with a 1:1 molar mixture of NaCl and KCl. The assembly was heated at 650-700 °C in air for 6-24 h in a muffle furnace. After cooling, the product was washed with an aqueous 0.1 M APS solution to remove residual Cu, then repeatedly centrifuged in Milli-Q water until the pH reached neutrality. The washed product was dried at 60 °C to obtain oxygen-rich $Ti_3C_2T_x$ MXene powder.

Materials characterization

1) The obtained Ti_3AlC_2 MAX phase and $Ti_3C_2T_x$ MXene powders were characterised for phase identification by X-ray diffraction (XRD). A Rigaku (Tokyo, Japan) diffractometer operating at 40 kV and 15 mA with a Cu Kα (λ ~ 1.5406 Å) X-ray source was used, with a scan range of 5° to 80° (2θ) and a step size of 0.02°.

2) Raman spectra were collected using a Renishaw InVia Micro Raman Spectrometer (Gloucestershire, U.K.) with a 50x objective, a 532 nm laser, and a 30-second acquisition time.
3) Morphological analysis (Field Emission Scanning Electron Microscopy) was performed using a JEOL JSM-1T800 microscope with a 15 kV beam and Energy-dispersive X-ray spectroscopy (EDS), including elemental mapping. The samples were prepared by sonication in Milli-Q water for ~1 h, then drop-cast onto silicon wafers.
4) Transmission Electron Microscopy (TEM) was performed using a JEOL JEM-2000F operated at 200 kV. All the samples were drop-cast onto carbon-coated copper grids for TEM analysis.
5) Dynamic light scattering (DLS) was used for particle size investigation of the catalysts using an Anton Paar Litesizer 500 particle size analyser.
6) Brunauer-Emmett-Teller (BET) surface area and pore size of the samples were measured using a Micromeritics (ASAP2020) system. Specific surface area was estimated from the N_2 adsorption-desorption isotherm obtained at 77 Kelvin.
7) Thermogravimetry and Differential Scanning Calorimetry (TGA and DSC) were analysed using a NETZSCH (STA449F3 Jupiter) system. All samples were prepared in an inert atmosphere over a temperature range from room temperature to 1200 °C.
8) X-ray photoelectron spectroscopy (XPS) was performed using a ULVAC-PHI 5000 Versa Probe III system with monochromatic Al K_α X-rays (1486.70 eV). XPS measurements were performed in an ultra-high-vacuum (UHV) chamber with a base pressure of $<6.75 \times 10^{-10}$ Torr. Casa XPS software was used for XPS peak fitting.

Phase purity calculation of Ti_3AlC_2 MAX phase and $Ti_3C_2T_x$ MXenes

The Ti_3AlC_2 MAX phase purity is calculated using a semi-quantitative formula as given below[36]

$$w_a = \frac{I_a}{(I_a+0.22I_b+0.084I_c)} \quad (10)$$

$$w_b = \frac{I_b}{(I_a+0.22I_b+0.084I_c)} \quad (11)$$

$$w_c = \frac{I_c}{(11.905I_a+2.619I_b+I_c)} \quad (12)$$

where w_a, w_b, *and* w_c represent the mass fractions of Ti_3AlC_2, Ti_2AlC, and TiC phases, respectively. I_a, I_b *and* I_c represent the integrated peak intensities of Ti_3AlC_2 (002) at $2\theta = 9.5^o$, Ti_2AlC (002) at $2\theta = 13^o$ and TiC (111) at $2\theta = 35.9^o$, respectively.

The phase purity of $Ti_3C_2T_x$ MXene is calculated from the following formula:

$$y = 1 - 0.2x + 0.013x^2 \quad (13)$$

where, y = weight fraction of Ti_3C_2 and x = intensity ratio of the Ti_3AlC_2 (104) at $2\theta = 39^o$ peak to the $Ti_3C_2T_x$ (002) peak.[16]

Phase purity was calculated by using the baseline-corrected XRD pattern. The XRD peak baseline was corrected in Origin 2018 to calculate peak intensities.

Electrochemical measurements

The electrochemical measurements were performed using a Metrohm Autolab PGSTAT302N electrochemical workstation in a standard three-electrode configuration. All chronoamperometric and cyclic voltammetry stability measurements were performed using an H-type electrochemical cell. The amounts of hydrogen generated from HER and oxygen generated from OER were quantified using a

Shimadzu Nexis GC-2030 (p-TCD) Gas Chromatograph. A two-electrode electrochemical cell was also used for water splitting experiments.

We have performed all electrochemical studies of the hydrogen evolution reaction (HER) and oxygen evolution reaction (OER) on the prepared $Ti_3C_2T_x$ MXene catalysts using a traditional three-electrode electrochemical cell setup. Electrochemical testing, including linear sweep voltammetry (LSV), cyclic voltammetry (CV), electrochemical impedance spectroscopy (EIS), and chronoamperometry for long-term stability assessment, was performed for the synthesised catalysts. For chronoamperometry measurements, we used an H-type electrochemical cell (Nafion 117 membrane) with each compartment of 50 ml capacity, filled with 20 ml of electrolyte (0.5 M H_2SO_4 or 1 M KOH), and purged with N_2 gas for 1 h to remove dissolved oxygen from the solution. A platinum sheet (Metrohm India Ltd.) was used as the counter electrode (CE), and a $Hg/HgCl_2$ (3 M KCl) was used as the reference electrode (RE). The $Ti_3C_2T_x$ MXene powder drop-cast onto Ni foam was used as the working electrode (WE). We prepared the working electrode by first cleaning the Ni foam (0.25 x 1 cm^2) in 3 M HCl for 15- 20 min, then in Milli-Q water until the pH was 6-7. Finally, acetone was used for washing via sonication, and the electrode was dried at 60 °C for 2 h in a vacuum oven before electrochemical measurements. A 0.5 mg MXene sample was dispersed in 100 µL of solvent (Milli-Q H_2O: isopropyl alcohol (IPA), 2:1), and 0.8 µL of Aquivion (25 %) binder was added to the solution. The catalyst ink was sonicated for 30 min at room temperature, and 25 µL of the as-prepared catalyst ink was drop-casted on the Ni foam and dried at 60 °C for 2 h in a vacuum oven. The catalyst mass loading was 0.625 mg cm^{-2}. All experiments were carried out at room temperature (23 °C). All the measured electrochemical potentials were converted to the reversible hydrogen electrode (RHE), using the Nernst equation:

$$E_{RHE} = E(Hg/HgCl_2) + (0.059 \times pH) + E^o (Hg/HgCl_2), \text{ where } E^o (Hg/HgCl_2) = 0.241 \text{ V} \quad (14)$$

Where E_{RHE} = potential relative to the Reversible Hydrogen Electrode
For 0.5 M H_2SO_4, E_{RHE} = 0.258 V; for 1 M KOH, E_{RHE} = 1.07 V.

- Before each electrochemical experiment, 30 full-cycle CVs at a scan rate of 100 mV s^{-1} were performed for all the samples for electrochemical surface cleaning.
- Linear sweep voltammetry (LSV) was performed at a scan rate of 5 mV s^{-1} for both HER and OER in 0.5 M H_2SO_4 and 1 M KOH. The potential window is fixed from 0 to -0.8 V vs RHE for HER and 1 to 2 V vs RHE for OER. All LSV curves for HER were corrected with 95% *iR* compensation in 0.5 M H_2SO_4 and 85% *iR* compensation in 1 M KOH to minimise the effect of solution resistance.
- Non-Faradaic CVs were carried out over a scan rate range of 5 – 120 mV s^{-1} to evaluate the ECSA.
- Electrochemical Impedance Spectroscopy (EIS) was performed at open circuit potential (OCP) over a frequency range of 0.1–100 kHz.

- The Tafel slopes were calculated by fitting the overpotential (η) versus log $|j|$ using the equation (η=a+b × log j), where η = overpotential, a = intercept of the slope, and b = Tafel slope

ECSA was estimated by measuring the double-layer capacitance within a non-Faradaic potential region, following the methodology. [50]

$$ECSA = \frac{C_{dl}}{C_S} \quad (15)$$

where C_{dl} (mF) is the double-layer capacitance of $Ti_3C_2T_x$ MXene and C_s is the theoretical specific capacitance (0.035 mF cm^{-2} for 0.5 M H_2SO_4 and 0.04 mF cm^{-2} for 1 M KOH).

The C_{dl} value was calculated from the CV non-faradic region by using the following formula.

$$C_{dl} = \frac{\Delta J}{2x\nu} \qquad (16)$$

where ΔJ is the difference in current density between anodic and cathodic sweeps (A), i.e., J_a - J_c. and ν = scan rate (V s^{-1}).

The roughness factor (RF) was calculated by following the formula

$$RF = \frac{ECSA}{GSA} \qquad (17)$$

where *GSA* = geometrical surface area. In this study, the GSA of Ni foam is 0.5 $cm^{2,}$ corresponding to the exposed area of the Ni foam as the working electrode.

Faradaic efficiency (FE): Faradaic efficiencies of the catalysts were determined using a gas chromatograph (GC) to quantify the H_2 and O_2 gases evolved during the electrochemical HER and OER reactions, thereby evaluating their catalytic performance. All measurements were conducted in the airtight H-type electrochemical cell. Upon completion of the HER and OER experiments, the evolved H_2 or O_2 gas was collected using a 100 µL airtight glass syringe and subsequently injected into the GC for quantitative analysis.
FE represents the fraction of the total charge consumed that contributed to H_2 or O_2 evolution and was compared with the theoretically expected H_2 or O_2 generation assuming 100% catalytic efficiency. The theoretical molar quantity of H_2 or O_2 was calculated from the accumulated charge during galvanostatic electrolysis using the following expression:

$$\textit{Theoretical amount (n in mole) of gas } (H_2 / O_2) = Q / (n * F) = (I * t) / (n * F) \qquad (18)$$

where I = applied current (A), t = electrolysis duration (s), n = 2 is the number of electrons transferred per molecule of H_2 in HER and O_2 in OER, and F = Faraday constant (96485.3 C mol^{-1}).

The Turnover Frequency (TOF): TOF represents the intrinsic catalytic activity and was calculated by the following formula:

$$TOF = \frac{j \times A}{2 \times F \times n} \qquad (19)$$

where $|j|$ = current density (A cm^{-2}), A = geometric area of the electrode (cm^2), F = Faraday constant (96485 C mol^{-1}), and n = number of active sites (mol). The TOF values are expressed in s^{-1}, representing the number of hydrogen or oxygen molecules generated per active site per second.

Data availability

Source data and additional data supporting this study are available from the corresponding authors and can be provided upon reasonable request.

References

50. McCrory, C. C. L., Jung, S., Peters, J. C. & Jaramillo, T. F. Benchmarking heterogeneous electrocatalysts for the oxygen evolution reaction. *J. Am. Chem. Soc.* **135**, 16977–16987 (2013).

Acknowledgement:

S.N., A.R., G.M., S.M. and S.S. acknowledge support from the CSIR-IMMT, India, (ULIP-EM; project MLP 002625). S.N. also acknowledges support from the Department of Science and Technology (DST), India, via the Start-up Research Grant. G.M. acknowledges the support from DST-INSPIRE; S.M. thanks DST-WISE for PhD fellowships. S.S. thanks the University Grants Commission (UGC) for a PhD fellowship.

Author Contributions:

S.N. conceived the idea. G.M. designed the experiments, performed materials synthesis and optimisation, and carried out characterisations, including XRD, Raman, SEM, TG-DSC, and surface area measurements. G.M., S.M., and S.S. performed all electrochemical measurements and data analysis. B.K.P. performed the XPS measurements, and G.M. and S.M. contributed to the analysis of the results. G.M. and A.R. contributed to the TEM measurements and data analysis. All the authors contributed to the analysis of the results and the interpretation of the data. G.M. and S.M. wrote the initial draft; A.R. and S.N. discussed all results and revised the manuscript; and S.N. wrote the final version with input from all authors.

Competing interests

The authors declare no competing interests.

Correspondence and requests for materials should be addressed to Ashutosh Rath or Simantini Nayak

Extended Data

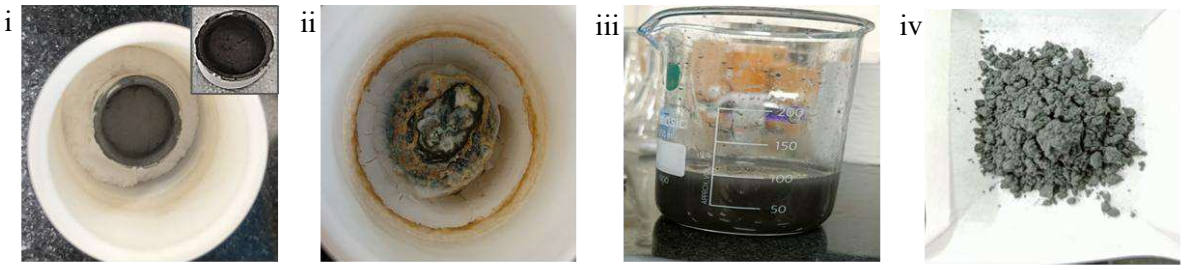

a. Ti_3AlC_2 MAX phase

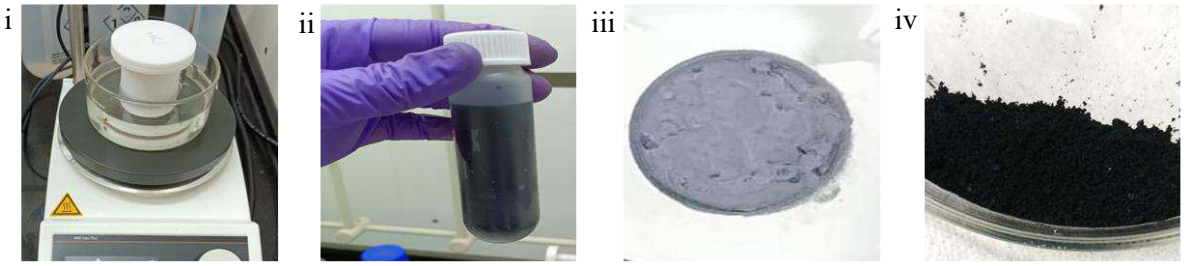

b. Ti_3C_2-F MXene

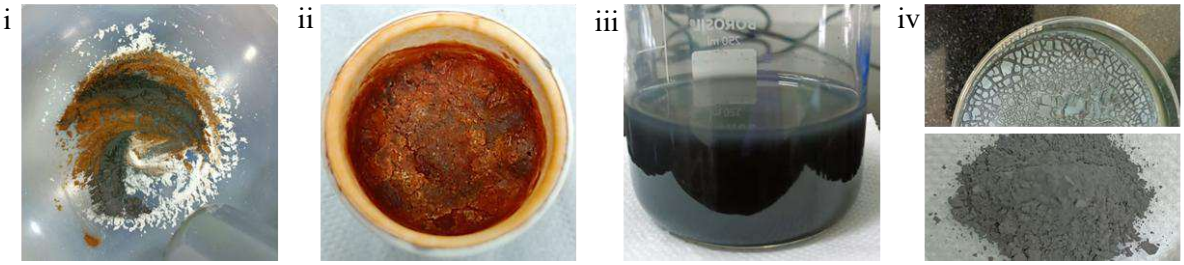

c Ti_3C_2-O MXene

Extended Data Fig. 1| a, Synthesis of the Ti_3AlC_2 MAX phase, i) Ti, TiC, Al mixture, ii) compact Ti_3AlC_2 MAX phase after sintering, iii) Ti_3AlC_2 MAX phase after washing and iv) Ti_3AlC_2 MAX phase after drying (powder); **b**, synthesis of Ti_3C_2-F MXene, i) *in situ* HF etching of Ti_3AlC_2 MAX phase, ii) and iii) Ti_3C_2-F MXene during and after washing, and iv) Ti_3C_2-F MXene powder; and **c**, synthesis of Ti_3C_2-O MXene, i) mixture of Ti_3AlC_2 MAX phase and molten salts ($CuCl_2$, NaCl and KCl), ii) after molten salt etching, iii) washing of Ti_3C_2-O MXene, and iv) Ti_3C_2-O MXene powder.

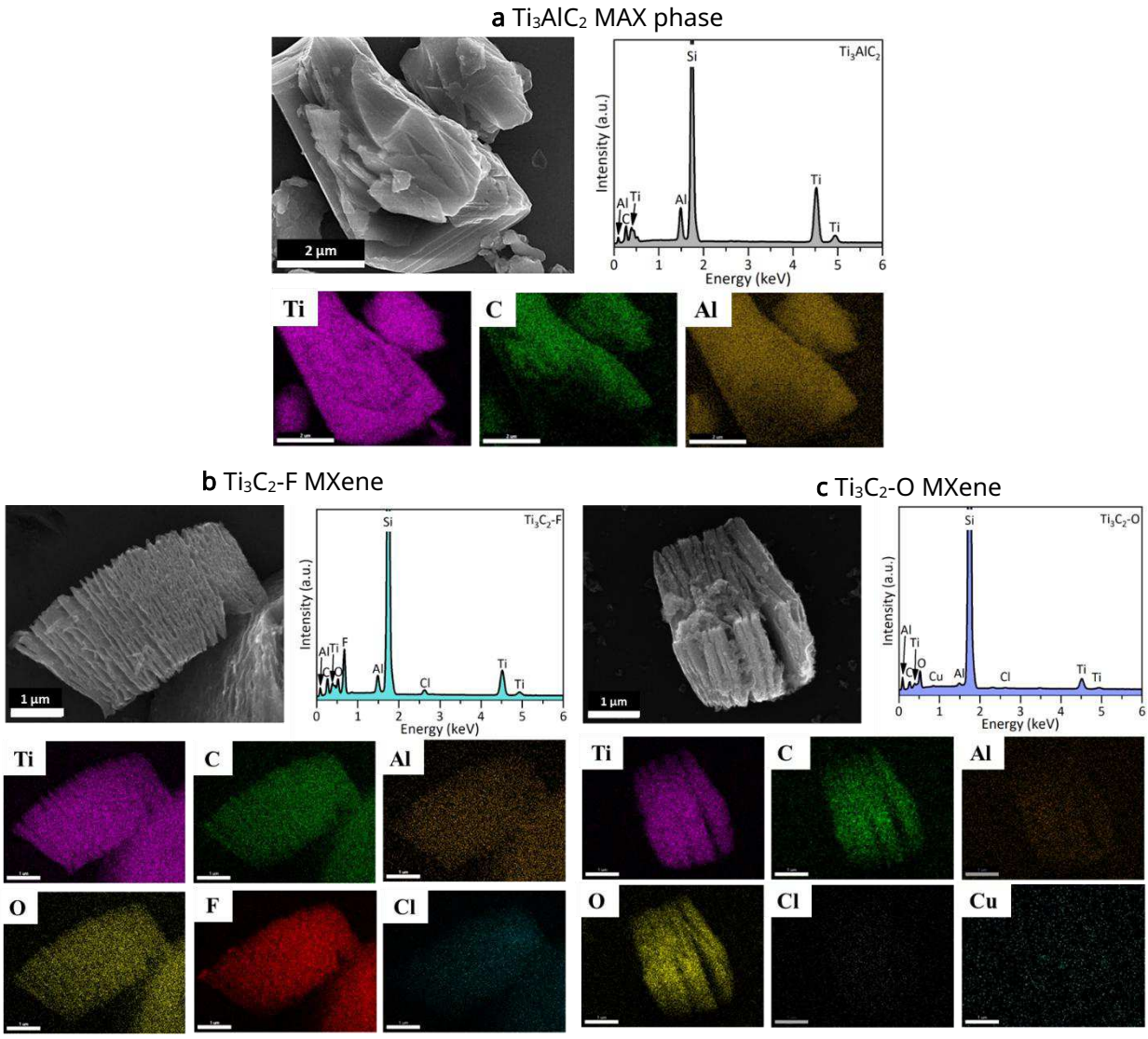

d

Element	Ti	Al	C	O	F	Cl	Cu
Ti_3AlC_2	30.7%	8.1%	61.2%	--	--	--	--
Ti_3C_2-F	9.0%	3.1%	41.8%	17.0%	28.2%	0.8	--
Ti_3C_2-O	10.0%	2.7%	33.5%	53.3%	--	0.2%	0.3%

Extended Data Fig. 2| SEM, elemental mapping and EDS characterisations of Ti_3AlC_2 MAX phase, Ti_3C_2-F and Ti_3C_2-O MXenes. a-c, SEM and elemental mapping images, EDS images. **d**, element ratios.

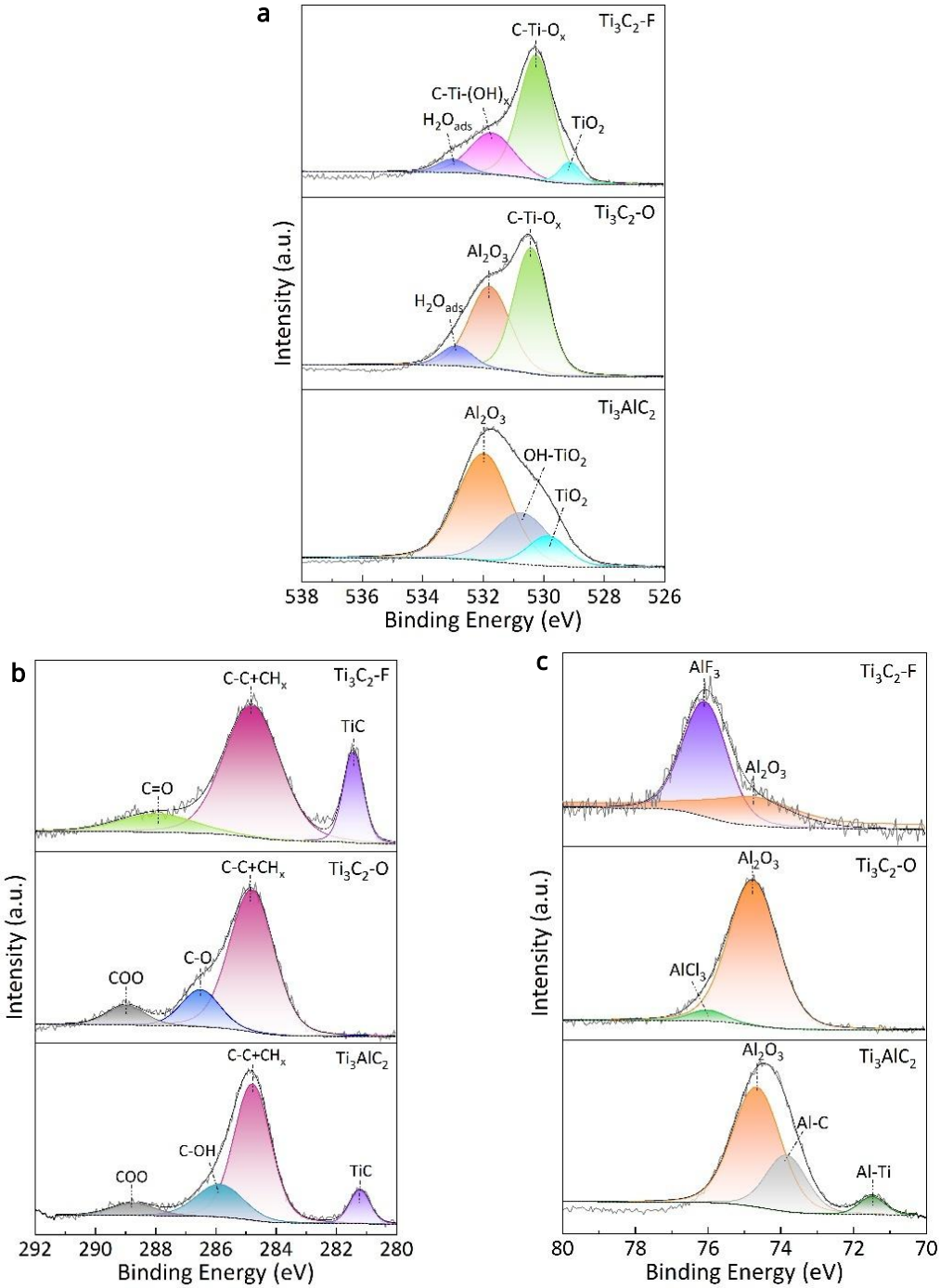

Extended Data Fig. 3| XPS characterisation of Ti_3AlC_2 MAX phase, Ti_3AlC_2 MAX phase, and $Ti_3C_2T_x$ MXenes. a, O 1s. **b**, C 1s. **c**, Al 2p.

Ti_3AlC_2 MAX phase										$Ti_3C_2T_x$ MXene			Ref.
Precursor (molar ratio)					Synthesis parameters				Purity (wt %)	Etching parameters		Purity (wt %)	
Ti	Al	TiC	TiH_2	C	Ball milling	Pelletisation	Sintering conditions Molten salt/ Temp./ Time/ Gas	Acid washing		Etchants/ temp./ time	Delamination		
--	1	1.8	1				(NaCl + KCl)/ 1050 °C/ 0.5 h/ Ar		98.5				37
3	1.1			2	10 h (Ar)		(NaCl + KCl)/ 1150 °C/ 2 h/ vacuum		99.0				36
3	1.5			1.9	10 h		(NaCl + KCl)/ 1250 °C/ 9 h/ Ar		97.8				38
3	1.2			2	10 h	yes	No salt/ 1300 °C/ 1.5 h/ Air		97.23				39
--	1.2	2	1		24 h		KCl/ 1200 °C/ 2 h/ Ar		98.5	$HF_{conc.}$/ RT/ 24 h	NaOH		44
3	1.5			1.9	12 h	yes	KBr/ 1350 °C/ 1.5 h/ Air		99	$HF_{40\%}$/ 50 °C/ 24 h			11
1.25	2.2	2			18 h		No salt / 1380 °C/ 2 h/ Ar	4 h (HCl)		(HCl + $HF_{50\%}$)/ 35 °C/ 24 h	LiCl		15
1.1	1.2	1.9					No salt/ 1510 °C/ 4 h/ Ar			(TMAF + HCl)/ RT/ 48 h, 120 h			33
3	1.1			1.8			No salt/ 1650 °C/ 2 h/ Ar		95	(LiF + HCl)/ RT/ 40 h			13
3.4	1.5			2	4.6 h		No salt/ 1450 °C/ 5 h/ Ar			(LiF + HCl)/ 50 °C/ 24 h			34
3	1.1			2	2 h	yes	No salt/ 1400 °C/ 3 h/ Ar			(LiF + HCl)/ 35 °C/ 24 h	LiOH		35
3	1			1.9	24 h	yes	KBr/ 1250 °C/ 5 h/ Air		94	(LiF + HCl)/ 40 °C/ 24 h	TBAOH		42
1.25	**2.2**	**2**					**NaCl + KCl/ 1300 °C/ 4 h/ Air**		**99.45**	**i. (LiF + HCl)/ 55 °C/ 24 h** **ii. $CuCl_2$/ 700 °C/ 12 h**		**99.71** **99.66**	**This work**

Extended Data Table 1| Comparison of the synthesis methods and phase purities of the Ti_3AlC_2 MAX phase and $Ti_3C_2T_x$ MXenes with those reported.

Supplementary Files

This is a list of supplementary files associated with this preprint. Click to download.

- SupportingInfoTerminationControlledPhasepureSNayak.docx